



Shifts in Phytoplankton Composition and Stepwise Climate Change During the Middle Miocene

J. Henderiks, M. Bartol, Nicolas Pige, B.-th. Karatsolis, B. Lougheed

► To cite this version:

J. Henderiks, M. Bartol, Nicolas Pige, B.-th. Karatsolis, B. Lougheed. Shifts in Phytoplankton Composition and Stepwise Climate Change During the Middle Miocene. *Paleoceanography and Paleoclimatology*, 2020, 35 (8), 10.1029/2020PA003915 . hal-04884998

HAL Id: hal-04884998

<https://hal.science/hal-04884998v1>

Submitted on 15 Jan 2025

HAL is a multi-disciplinary open access archive for the deposit and dissemination of scientific research documents, whether they are published or not. The documents may come from teaching and research institutions in France or abroad, or from public or private research centers.

L'archive ouverte pluridisciplinaire **HAL**, est destinée au dépôt et à la diffusion de documents scientifiques de niveau recherche, publiés ou non, émanant des établissements d'enseignement et de recherche français ou étrangers, des laboratoires publics ou privés.



Distributed under a Creative Commons Attribution 4.0 International License

Paleoceanography and Paleoclimatology

RESEARCH ARTICLE

10.1029/2020PA003915

Special Section:

The Miocene: The Future of the Past

Key Points:

- A major cooling step during the middle Miocene impacted phytoplankton communities across high and low latitudes in the Atlantic Ocean
- Onset of “icehouse world” saw an increase in abundance and diversification of alkenone-producing haptophyte algae
- The middle Miocene Climate Transition was a significant step toward establishing modern ocean circulation and phytoplankton communities

Supporting Information:

- Supporting Information S1

Correspondence to:

J. Henderiks,
jorijntje.henderiks@geo.uu.se

Citation:

Henderiks, J., Bartol, M., Pige, N., Karatsolis, B.-T., & Lougheed, B. C. (2020). Shifts in phytoplankton composition and stepwise climate change during the middle Miocene. *Paleoceanography and Paleoclimatology*, 35, e2020PA003915. <https://doi.org/10.1029/2020PA003915>

Received 24 APR 2020

Accepted 17 JUL 2020

Accepted article online 22 JUL 2020

Shifts in Phytoplankton Composition and Stepwise Climate Change During the Middle Miocene

J. Henderiks¹ , M. Bartol¹ , N. Pige^{1,2}, B.-Th. Karatsolis¹ , and B. C. Lougheed¹ 

¹Department of Earth Sciences, Uppsala University, Uppsala, Sweden, ²Laboratory of Geology of Lyon: Earth, Planets and Environments (LGLTPE), Université Claude Bernard Lyon 1, ENS de Lyon, Villeurbanne, France

Abstract The abundance and composition of modern phytoplankton are primarily related to equator-to-pole temperature gradients and global ocean circulation, which in turn determine the availability of nutrients in the photic zone. The nutricline is found at greater depths in warm, tropical waters, whereas more vigorous surface mixing in higher latitudes (seasonally) enhances nutrient availability and primary productivity. Ocean temperatures were $\sim 7^{\circ}\text{C}$ higher during the middle Miocene Climatic Optimum (MCO; ~ 16.9 – 14.7 million years ago, Ma), which was followed by Antarctic glaciation and global cooling during the middle Miocene Climate transition (MMCT; 14.7 – 13.8 Ma). Four decades ago, Haq (1980, <https://doi.org/10.2307/1485353>) already related migration patterns of low-latitude versus high-latitude calcareous nannoplankton in the Atlantic Ocean to major climatic fluctuations during the Miocene. Here, we detail and discuss the macroevolutionary patterns and processes across the middle Miocene (~ 16.5 – 11 Ma) at five deep sea sites on a north-south transect in the Atlantic Ocean (57°N to 28°S). We show that the major cooling step toward the modern “icehouse” world impacted coccolithophore communities at all latitudes. Contrary to previous observations suggesting that tropical sites showed little change and that midlatitudes were the most sensitive recorders of climate change across the MMCT, we show that all sites recorded a marked diversification and increase in abundance of reticulofenestrids. Global cooling and related increased meridional overturning circulation are implicated as likely forcings for this macroevolutionary step toward establishing modern coccolithophore communities that are dominated by eurythermal and eurytrophic species such as *Emiliania huxleyi*.

Plain Language Summary How will marine plankton communities respond to a much warmer world than today? How fast or slow would such changes be? We can learn valuable lessons from the fossil record of coccolithophores that represent a prominent phytoplankton group in both past and modern oceans. Changes in the composition of fossil assemblages show that species tracked past climate change on submillion year scales in the Atlantic Ocean. When ocean temperatures were $\sim 7^{\circ}\text{C}$ warmer during the middle Miocene (~ 16 million years ago), tropical species reached into the midlatitudes (42°N) of the North Atlantic. When the Antarctic ice sheet grew larger and the oceans cooled after ~ 14.7 million years ago, a group known as the reticulofenestrids diversified and became the most common everywhere, also in the tropics. Apparently, this group maintained high fitness in an “icehouse” world with greater latitudinal temperature contrasts, more vigorous ocean circulation, and higher nutrient availability in the photic zone. Indeed, their cosmopolitan distribution implies broad temperature and other environmental tolerances, similar to the group’s latest descendant, the modern species *Emiliania huxleyi* that also displays a wide genetic and ecophenotypic diversity.

1. Introduction

The physicochemical properties of the surface oceans (including sea surface temperature, light, and nutrient availability) directly influence marine photosynthetic algae and primary productivity. Climate change can significantly contribute to changes in the abundance and composition of phytoplankton communities, which, in turn, affect global biogeochemical cycles. Rising ocean temperatures (Levitus et al., 2005) affect ocean circulation and the physical properties of the surface water and will likely cause poleward shifts in phytoplankton thermal niches (Thomas et al., 2012). A warmer, more stratified water column reduces the nutrient input into upper water layers, increasing the likelihood of nutrient limitation in algae (e.g., Sarmiento et al., 2004). Marine algae that are able to sustain photosynthesis and growth under low-nutrient concentrations, such as the coccolithophores (calcifying haptophytes), are expected to

©2020. The Authors.

This is an open access article under the terms of the Creative Commons Attribution License, which permits use, distribution and reproduction in any medium, provided the original work is properly cited.

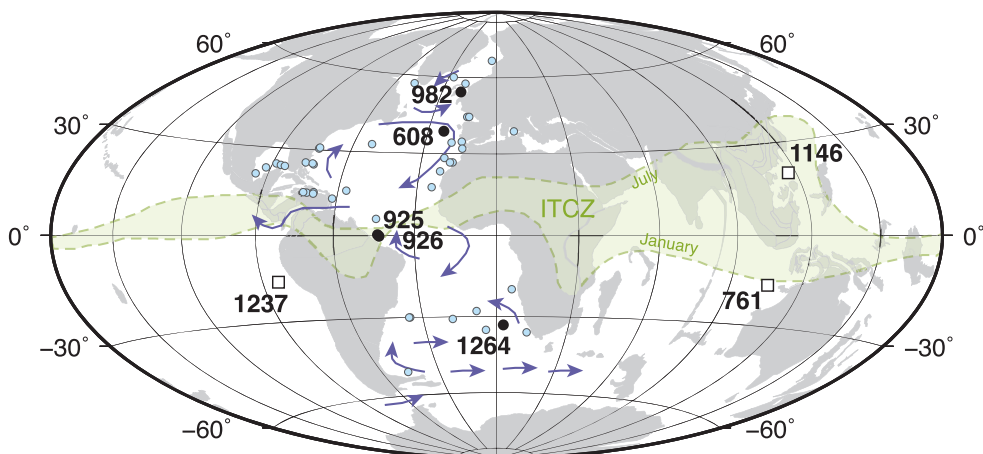


Figure 1. Paleogeographic reconstruction for the middle Miocene (15 Ma; www.odsn.de) and locations of DSDP and ODP sites. North-South Atlantic deep sea coring transect detailed herein (black circles), DSDP sites studied by Haq (1980) (light blue circles), and other relevant ODP sites discussed in this study (open squares). Also shown are the main Atlantic surface circulation patterns modeled for this time interval (blue arrows; cf. Herold et al., 2012) and the modern, seasonal extent of the ITCZ (green shaded area).

perform better under such conditions (e.g., Gerecht et al., 2014; Šupraha et al., 2015) than, for example, diatoms (e.g., Lazarus et al., 2014). In order to better understand the long-term impacts of such ecological shifts, we need to study the fossil record of past warm climates.

Haq (1980) published a pioneering synthesis of Miocene nannofossil census data collected from 43 different Atlantic deep sea sites (DSDP Legs 1–47; Figure 1). The broad-scale paleobiogeographic patterns that he reconstructed for six Miocene time slices (of ~0.5 million-year duration each) provided fundamental insights that remain valid today. At the time, Haq (1980) stated that “the history of the Miocene climatic variations in [the Atlantic] ocean, as interpreted from the faunal and isotopic records is still sketchy” and “temporal migration patterns of nannoplankton should provide a more complete picture of climatic variations and the differences between the Northern and Southern Hemisphere climates”. Assuming species habitat tracking (migrations) as the main tool to reconstruct past environments, he identified several “warm” (poleward migration of low-latitude taxa) and “cool” (equatorward migration of high-latitude taxa) climate states, predominately recorded at midlatitudes of the North Atlantic (25–35°N).

Four decades later, we have gained much knowledge about Miocene climatic variations, even if many scientific challenges remain (as highlighted in this Special Section, *The Miocene: The Future of the Past*, [https://agupubs.onlinelibrary.wiley.com/doi/toc/10.1002/\(ISSN\)1944-9186.Miocene1](https://agupubs.onlinelibrary.wiley.com/doi/toc/10.1002/(ISSN)1944-9186.Miocene1)). A number of key paleoclimate proxy records, including those from the Atlantic Ocean, detail changes in ocean temperatures, ice volume, and past levels of atmospheric CO₂. The middle Miocene Climatic Optimum (MCO; ~16.9–14.7 Ma) was the warmest time interval of the Neogene, associated with a global perturbation of the carbon cycle (e.g., Diester-Haass et al., 2009; Holbourn et al., 2007), followed by significant surface ocean cooling of 6–7°C (Savin et al., 1985; Shevenell et al., 2004; Super et al., 2018) and Antarctic ice sheet growth during the middle Miocene Climate Transition (MMCT; 14.7–13.8 Ma) (Flower & Kennett, 1993, 1994; Holbourn et al., 2005). The MMCT is also associated with a moderate (~60–125 ppmv) decrease in atmospheric CO₂ levels (Badger et al., 2013; Super et al., 2018). Thus, the middle Miocene is a well-studied time interval with a range of geochemical and paleontological climate constraints (Figure 2). In addition, we have a much better understanding of coccolithophore ecology in relation to physical properties of the surface ocean, based on modern plankton observations (e.g., Baumann et al., 2005; Haidar & Thierstein, 2001) and nannofossil assemblage patterns in sediment traps and recent surface sediments (e.g., Boeckel et al., 2006; Broerse et al., 2000).

This study presents five new records of nannoplankton change across the middle Miocene (~16.5–11.5 Ma) along a north-south transect in the Atlantic Ocean (57°N to 28°S; Figure 1). By investigating all records within the same consistent analytical and geochronological framework, we are able to constrain both latitude-specific and ocean-wide common biotic response patterns in relation to global climate cooling across the MMCT. In combination with independent paleoclimate proxy records, this is an opportunity to test (1)

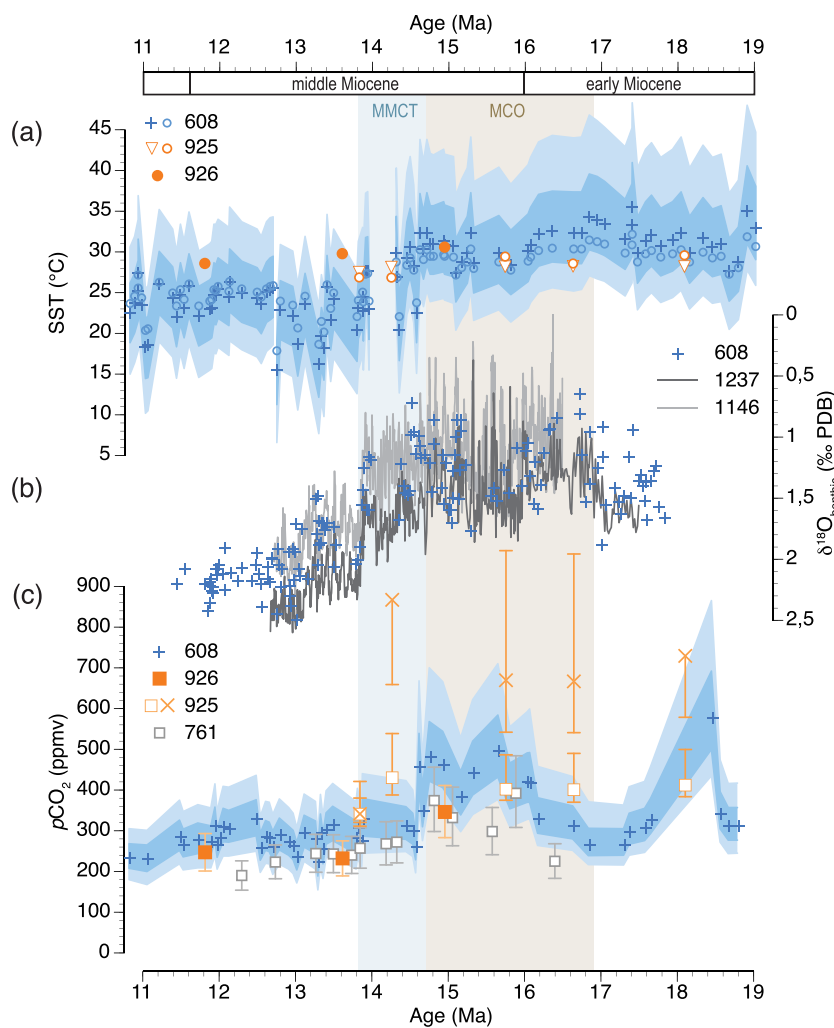


Figure 2. Overview of Miocene paleoclimate proxy records for selected Atlantic deep sea sites. (a) Sea surface temperature reconstructions. TEX₈₆-based SST estimates at North Atlantic DSDP Site 608 (blue shadings are 68% and 95% confidence intervals [CI]; Super et al., 2018); at Ceara Rise, ODP Sites 925 and 926 (orange), SST estimates are based on TEX₈₆ (open circles) or U k' ₃₇ (triangles) (Zhang et al., 2013) and Mg/Ca (closed circles) (Foster et al., 2012). (b) High-resolution benthic foraminiferal $\delta^{18}\text{O}$ records from the eastern equatorial Pacific (ODP Site 1237) and South China Sea (ODP Site 1146) that served to define the durations of the MCO and MMCT (indicated by shadings; Holbourn et al., 2005, 2007), overlain by benthic foraminiferal $\delta^{18}\text{O}$ measured at Site 608 (Diester-Haass et al., 2009; Wright et al., 1992). (c) Compilation of alkenone-based paleo- pCO_2 estimates at Site 608 (Super et al., 2018; blue shadings are 68% and 95% CI), ODP Site 925 (Zhang et al., 2013; squares: diffusive model calibration; crosses: recalculated, statistical model estimates by Stoll et al., 2019), and boron isotope-based estimates at ODP Sites 926 and 761 (Foster et al., 2012). See original publications for error estimates.

whether phytoplankton compositions indeed track climate change on sub-Myr scales, as well as how—through migrations, species replacement, or speciation and extinction events—and (2) how changes in pole-to-equator temperature gradients may have affected macroevolutionary turnover patterns in middle Miocene coccolithophore communities.

2. Materials and Methods

2.1. Deep Sea Sites and Age Models

The Deep Sea Drilling Project (DSDP) and Ocean Drilling Program (ODP) sites used in this study are listed in Table 1. Together, these sites cover a north-south transect across the Atlantic Ocean (Figure 1) that has been previously subject to similar latitudinal and interhemisphere comparisons (e.g., Diester-Haass et al., 2009)

Table 1
Site Locations and Sampling Details

| Site | Location | Latitude | Longitude | Water depth (m) | Samples (N) | A1-min (Ma) | A1-max (Ma) | Approx. sampling resolution (kyr) |
|-------|-----------------|-------------|-------------|-----------------|-------------|-------------|-------------|-----------------------------------|
| 982B | Rockall Plateau | 57°31,002'N | 15°51,993'W | 1,134 | 47 | 11.248 | 15.898 | 100 |
| 608 | King's Trough | 42°50,205'N | 23°5,252'W | 3,526 | 47 | 11.368 | 16.630 | 115 |
| 925A | Ceara Rise | 4°12,249'N | 43°29,334'W | 3,042 | 15 | 11.256 | 16.732 | 240 |
| 925B | Ceara Rise | 4°12,248'N | 43°29,349'W | 3,041 | 9 | | | |
| 926A | Ceara Rise | 3°43,146'N | 42°54,489'W | 3,598 | 42 | 11.725 | 16.446 | 115 |
| 1264A | Walvis Ridge | 28°31,961'S | 2°50,731'E | 2,507 | 16 | 11.530 | 16.091 | 70 |
| 1264B | Walvis Ridge | 28°31,950'S | 2°50,729'E | 2,504 | 57 | | | |

Note. Samples from multiple holes (Sites 925 and 1264) were combined on the composite depth below seafloor scale (mcd) before age model construction. A1-min = youngest sample age; A1-max = oldest sample age as derived from age-depth model A1, reported in Ma (note that *Undatable* output is in ka); ages and average sampling resolution given per site in case multiple holes were sampled.

and where several key paleoclimate proxy records have been produced for the targeted Miocene interval (Figure 2).

The northernmost location, ODP Site 982 was cored on the Rockall Plateau in the Hatton-Rockall Basin, where this site is bathed in North Atlantic Intermediate Water (NAIW). Middle to late Miocene sediments are dominated by biogenic carbonate, mainly nannofossil oozes and chalks (average $92.6 \pm 1.5\%$ carbonate content; Jansen et al., 1996). On the southern flank of the King's Through, DSDP Site 608 underlies the northern part of the modern North Atlantic subtropical gyre, and Miocene sediments are predominantly white nannofossil chalks (Ruddiman et al., 1987). There is a minor hiatus between cores 608-33X and 34X (Diester-Haass et al., 2009), as well as gaps in the sedimentary sequence at core breaks. However, this does not preclude our aim of assessing sub-Myr trends in nannofossil composition and abundance. At tropical latitudes in the western equatorial Atlantic, ODP Sites 925 and 926 were recovered along a depth transect on Ceara Rise (Curry et al., 1995) and are composed of nannofossil chalks with foraminifers alternating with clayey nannofossil chalks on a meter scale. In these sequences, carbonate content varies between 60% and 80% (Diester-Haass et al., 2009). The southernmost location on our transect, ODP Site 1264, was recovered from Walvis Ridge in the South Atlantic and is characterized by an alternation of nannofossil ooze and foraminifer-bearing nannofossil ooze on a decimeter to meter scale (Leg 208 Shipboard Science Party, 2004).

For each site, we constructed age models based on compilations of available shipboard data, previous high-resolution nannofossil studies, and geomagnetic reversal ages (Text S1 and Tables S1–S5 in the supporting information). Here, we use the *Undatable* MatLab age-depth modeling software Version 1.1 (Louheed & Obrochta, 2019), which incorporates uncertainty in both depth and age. Age error estimates (in kyr) are based on those determined for selected nannofossil bioevents (Backman & Raffi, 1997; Backman et al., 2012; Lourens et al., 2004; Zeeden et al., 2013); otherwise, we assumed a ± 100 kyr error. The depth error (in cm) is based on sample spacing between the (bio)stratigraphic events as reported in the literature or documented in this study. *Undatable*'s deterministic routines (with a positive sedimentation rate prior and bootstrapping) result in median and mean age-depth models, with age error estimates (nonnormally distributed 68% and 95% percentiles). Age-depth uncertainty in *Undatable* increases with increasing distance from age-depth determinations, thus including sedimentation rate uncertainty in the age-depth model, unlike linear age-depth models where sedimentation rate is assumed to be constant between age-depth determinations. This approach allows us to make informed intersite comparisons by taking geochronological uncertainty into account.

We developed two alternative age models for each site, Models A1 and A2 (Text S1; Figures S1 and S2). In the first, A1 (Figure S1; Tables S2 and S3), we applied calibrated ages for bioevents and geomagnetic reversals as compiled in the GTS of Gradstein et al. (2012), which, for the Miocene, are predominantly based on the Astronomically Tuned Neogene Time Scale 2004 (ATNTS2004) of Lourens et al. (2004) with updates by Hilgen et al. (2012). An alternative model, A2 (Figure S2; Tables S4 and S5), considered the full range of available bioevent age calibrations (Backman & Raffi, 1997; Backman et al., 2012; Lourens et al., 2004; Raffi et al., 2006; Zeeden et al., 2013) and higher age errors. Where available, a mean age was calculated from different calibrations ($N = 2$ to 5), and the standard deviation served as input for the age error. Because there are no interpretative consequences to using either Model A1 or A2, we present the results on the A1 model

only. Previously published paleoproxy records were updated to the same age-depth models for consistent comparisons.

2.2. Calcareous Nannofossil Counts

The composition of calcareous nannofossil assemblages can be significantly altered by differential dissolution (e.g., Lohmann & Carlson, 1981; Ruddiman & Heezen, 1967) and therefore bias census counts to common and dissolution-resistant taxa (Young et al., 2005). Middle Miocene deep sea records have been impacted by dynamic fluctuations of the calcite lysocline, especially during the MCO and in the Equatorial Pacific where it shoaled by 600 m (e.g., Kochhann et al., 2016; Pälike et al., 2012). Unconformities and dissolution events have been recognized at multiple Miocene sites, and bulk carbonate contents of <85 wt.% may indicate substantial dissolution within pelagic chalks (e.g., Woodruff & Savin, 1991). For the Atlantic records investigated here, we rely on several lines of evidence for relatively stable, moderate-to-good carbonate preservation.

Calcareous nannofossil preservation was assessed with a variety of quantitative and qualitative methods (Text S2 and Figure S3). We conclude, as previous authors have done before (e.g., Backman & Raffi, 1997; Gartner, 1992), that nannofossils are abundant throughout with good-to-moderate preservation (i.e., slight etching but no diagnostic structural changes) across the investigated middle Miocene time interval. However, except for Site 982, most sites reveal indications for higher levels of etching or selective dissolution of the smallest coccoliths during the MCO and across the MMCT (Text S2). Independent data on foraminiferal fragmentation and bulk carbonate content (Diester-Haass et al., 2009) support these observations (Figure S3). Nevertheless, we conclude that the compositional data presented herein reliably record variations in common and dissolution-resistant taxa within coccolithophore communities of the middle Miocene, even if selective dissolution had removed other (often rare), more susceptible species.

We sampled at ~100 kyr resolution (Table 1) in order to detect sub-Myr paleoecological and macroevolutionary trends based on nannofossil census counts. A total of 233 samples were counted under a polarized light microscope (Olympus and Zeiss Axioskop 40) at 1,000X magnification. Microscope slides were prepared from dried bulk sediments with the “drop technique” (Bordiga et al., 2015), which renders evenly distributed particles on the slide. It also allows for calculation of the absolute number of coccoliths per gram of sediment (N/g), with a reproducibility of ±10–15%. Coccolith concentrations can be converted into burial rates (or fluxes; N/cm² kyr) when mass accumulation rates are calculated (subject to age model errors; e.g., Suchéras-Marx & Henderiks, 2014).

Nannofossil assemblage compositions (in %) were quantified by counting at least 300 specimens determined to species or genus level. Samples from Sites 982, 608, 925, and 926 were counted at the species level, whereas counts at Site 1264 considered genus level only. In total, 69 morphospecies from 22 genera were observed; 50 morphospecies were recombined into nine genus-level groups, and 19 other subordinate taxa were lumped as “others” in the genus-level multivariate analyses (see taxonomic list in Table S6). The degree of calcification of the central area of the reticulofenestrids (ancestry of modern *Emiliania huxleyi* and *Gephyrocapsa oceanica*; Noelaerhabdaceae family) was distinguished in the genus-level groupings with a heavily calcified (*Reticulofenestra* closed) and less heavily calcified (*Reticulofenestra* open) category (Text S3). The 95% confidence intervals (95% CI) for the relative abundance estimates were calculated in PAST Version 3.20 freeware (Hammer et al., 2001; Suchéras-Marx et al., 2019).

Haq (1980) reconstructed long-term biogeographic patterns in the Atlantic based on census counts of 17 taxonomic groups (cf. Table S6); we included part of this published database in our comparative analyses. The selected data, covering the time interval 17–11 Ma and including 130 samples from 25 sites (DSDP Legs 2–47), were subdivided into 1 Myr time bins (cf. Figure 2 in Haq, 1980) and grouped in different geographic regions: northern North Atlantic >45°N, North Atlantic (30–45°N, including Mediterranean), (sub)tropical North Atlantic (0–30°N; including four subregions in the northern and southern Caribbean; eastern and western Atlantic), South Atlantic (30–45°S), and southern South Atlantic >45°S (single site, DSDP Site 329).

2.3. Statistical Analyses

For the sites with species-level counts, indices of fossil species diversity (based on full assemblages as well as within the reticulofenestrids [Noelaerhabdaceae] only) were calculated using PAST Version 3.20 freeware

(Hammer et al., 2001). A single PAST diversity analysis (bootstrapped, $N = 9,999$) renders 12 different indices, but here we only discuss Shannon diversity (H), which is an index accounting for both the number and evenness of the species. The same software was used to explore the multivariate census data with statistical ordination techniques, as explained in more detail below.

2.3.1. Multivariate Ordination

We applied detrended correspondence analysis (DCA; Hill & Gauch, 1980) to visualize the biogeographic groupings and temporal trends of the 233 multivariate samples from five sites. In DCA, compositional data (in %) can be analyzed without modification, which results in an ordination of both taxonomic data and samples (Hammer & Harper, 2006); in other words, it distinguishes assemblages between sites and temporal trends at each individual site. Canonical correspondence analysis (CCA; Ter Braak, 1986) adds the possibility to investigate the relationships between the fossil assemblages and their environment. We applied CCA with latitude and longitude (biogeography) as well as sample age (time; macroevolution) as environmental variables. DCA and CCA give eigenvalues, indicating the percent of the total correlation between the species and samples captured by each axis. However, no measures of statistical significance are calculated, and both ordination methods mainly serve to summarize the main trends within the multivariate data set(s). The statistical significance of trends is subsequently tested on (selected) raw input data and their respective error estimates.

2.3.2. Lumping or Splitting Taxonomy?

Because we had no *a priori* hypotheses regarding what taxonomic level would underpin major temporal and biogeographic trends, we performed 19 runs with either species ($n = 69$) or genus ($n = 10$) level counts, on individual sites and all sites combined (Table S7). Note that CCA was only run on combinations of multiple sites. To facilitate comparison between the results of DCA runs on individual sites (e.g., Runs 1–4 and 7–11), we standardized the sample scores (shown herein as time series) using the z score:

$$z_i = \frac{x_i - \bar{X}}{s}, \quad (1)$$

where x_i is the individual sample score, X the average, and s the standard deviation, of all sample scores within one time series (site). We also investigated the subset of the Haq (1980) database to inform our hypotheses (Runs 5 and 18), using his original taxonomic groupings ($n = 17$) as well as recombined into nine genus groups (*Helicosphaera* spp. included within “others” in this case; Table S6). In his original Q-mode Varimax Factor Analysis, Haq (1980) lumped discoasters, sphenoliths, and small reticulofenestrids but distinguished heavily calcified reticulofenestrids (*Dictyococcites* spp.) at species level. Genus groupings proved most straightforward in comparing our and Haq’s data sets (DCA and CCA Run 19). To track the intrageneric diversity in the most common placolith-bearing taxa, we adhered to size-defined morphospecies in *Coccolithus* and the reticulofenestrids (Text S3).

3. Macroevolutionary Trends and Biogeographic Patterns in Phytoplankton Communities

3.1. Temporal Trends in Nannofossil Census Data

Total nannofossil concentrations (N/g) are comparable between sites and show a slight increasing trend over time (Figure 3a). Average values ($4.8 \pm 1.9 \cdot 10^9$ liths/gram at Ceara Rise sites 925 and 926; $7.1 \pm 1.8 \cdot 10^9$ liths/gram at the other sites) confirm the pelagic character of all investigated oceanographic settings and suggest only few distinct fluctuations in dilution, dissolution, or nannofossil burial rates. Higher dilution with clays from the Amazon River may explain both lower bulk carbonate and nannofossil content at the Ceara Rise sites (Figure S3; Diester-Haass et al., 2009).

All records also reveal long-term, gradual changes in nannofossil composition as expressed by the standardized scores of DCA Axis 1 (Figure 3b). Whether analyzed at the species or genus level (Figure S4), each site individually demonstrates that MCO assemblage compositions were distinctly different from those after the MMCT—driven by changes in locally prominent taxa at each site (see section 3.2). The taxa that are consistently and most strongly related to DCA Axis 1 include *Cyclicargolithus floridanus*, *Sphenolithus heteromorphus*, *Discoaster* spp., and *Helicosphaera* spp. (the latter only at the tropical sites), versus large-sized and heavily calcified reticulofenestrids (*R. pseudoumbilicus* and *R. gelida*) on the opposite side of the scoring scale.

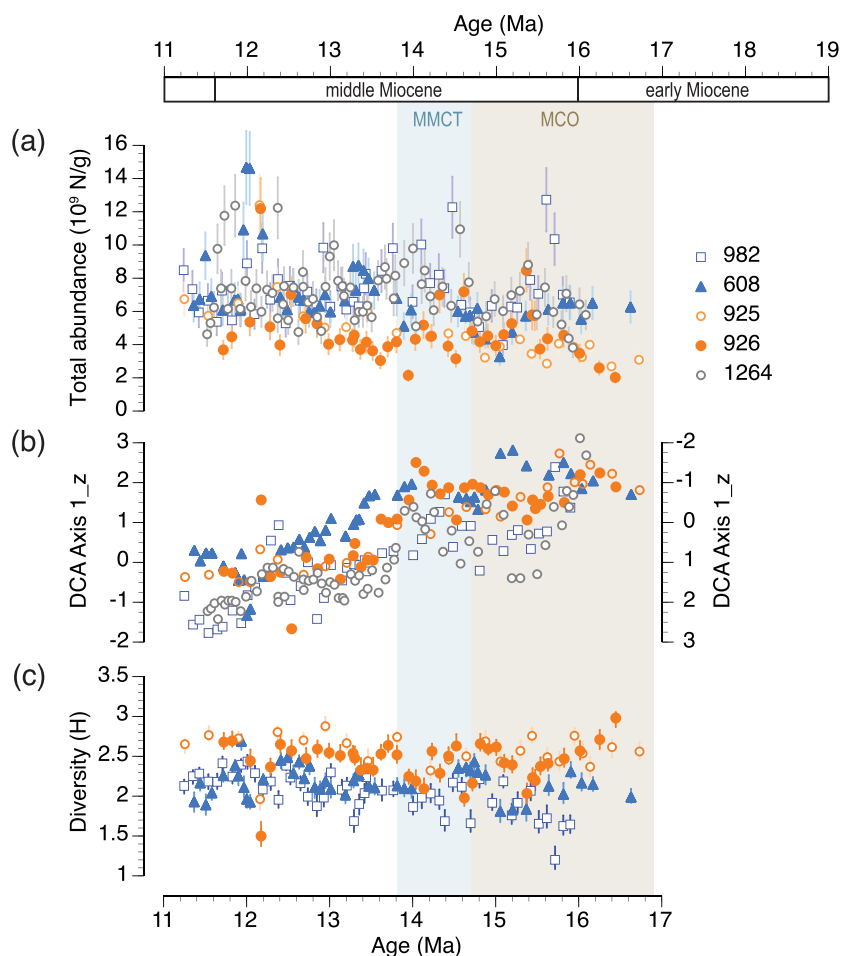


Figure 3. Long-term trends in calcareous nannofossil time series data. (a) Total nannofossil abundance (10^9 N/g), error bars $\pm 15\%$. (b) Site-specific temporal trends as expressed by DCA Axis 1 results from runs using all species % (Sites 982, 608, 925, and 926; Runs 1–4) or genus % data (Site 1264; Run 11) as input. Axis 1 scores were standardized for site-to-site comparisons. Note inverse scale (right y axis) for Sites 608, 925, and 926. (c) Shannon diversity index (H) based on species-level census counts (all sites except Site 1264); error bars are bootstrapped maximum and minimum estimates. Shadings indicate MCO and MMCT as in Figure 2.

On the other hand, no significant trends in total species diversity are observed over the investigated time interval (Figure 3c). Nevertheless, species diversity indices are consistently highest in the tropics (more rare taxa present) compared to the higher northern latitudes (no species-level diversity data available at Site 1264).

3.1.1. Evaluation of Site-to-Site Correlations

Our data analyses are made within the framework of a consistent age-depth approach for all sites that fully incorporates error in both age and depth, thus allowing evaluation of the site-to-site correlations based on statistical confidence intervals (Figure 4). This comparison illustrates that the nannofossil records serve to discuss long-term, sub-Myr scale trends and differences in composition across the MCO (roughly corresponding to nannofossil biozone NN4), MMCT (encompassed by biozone NN5), and “icehouse” phases (biozones NN6–NN7), rather than to pinpoint and correlate specific “events” in biotic change. Nevertheless, an independent, astronomically tuned age model for Site 1264 (Lourens et al., personal communication 2020, 3/2/2020; overlay in Figure 4) confirms the good sample age constraints across the MMCT and the younger part of the record. For the older part of the 1264 record, our age model relies on shipboard biostratigraphic tie points beyond our sampling interval, so it is hard to say what causes the “accordion” effect. However, this age model discrepancy has no impact on the main analyses and interpretations presented herein.

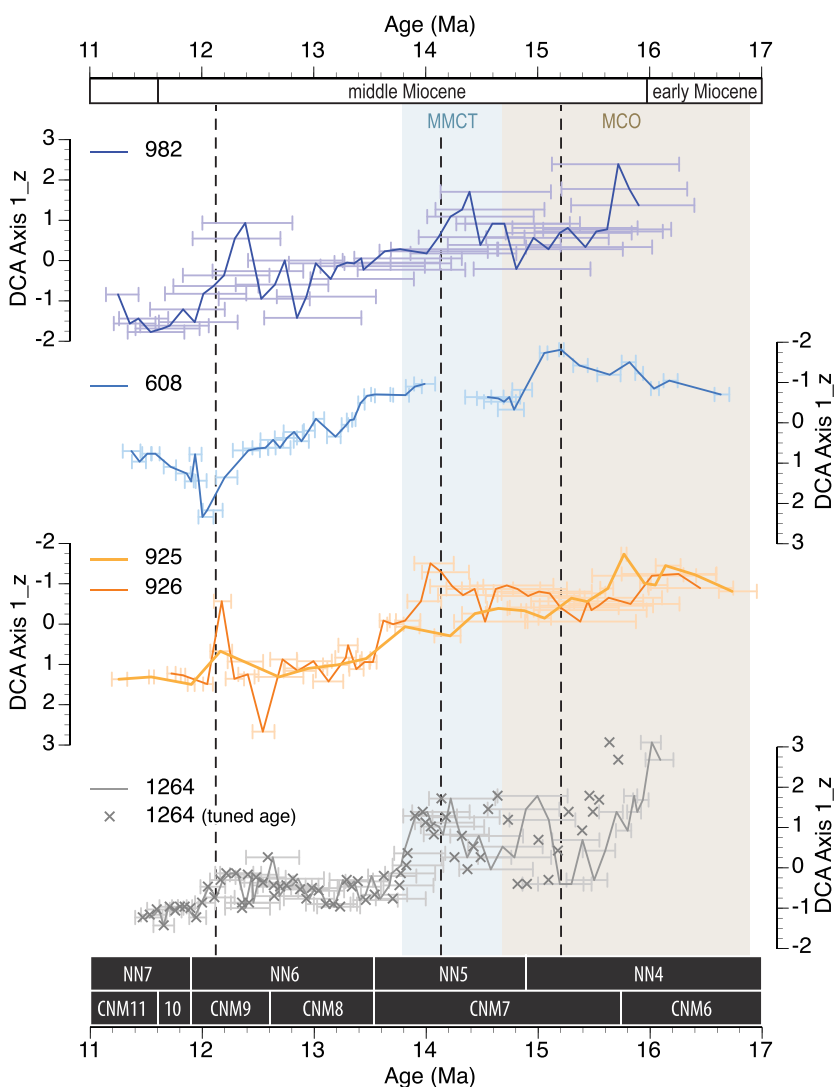


Figure 4. Time series of site-specific DCA sample scores (Runs 1–4 and 11; standardized values), showing long-term directional change within fossil assemblages at all sites. Sample median age (A1) and 68.2% range (entire width of error bar) are indicated to better evaluate site-to-site correlations. Vertical dashed lines serve as guides, rather than to highlight any specific event. Crosses in bottom panel indicate tuned sample ages at Site 1264 (L. Lourens, pers. comm. 2020). MCO and MMCT shadings as in previous figures; Neogene calcareous nannofossil biozonations cf. Martini (1971) (NN zonation) and Backman et al. (2012) (CNM zonation).

3.2. Biogeographic Contrasts in Species Composition

When combining genus-level compositional data from all sites, CCA (Run 12) confirms rather stable biogeographic patterns. It separates the South Atlantic site (1264) from the rest and characterizes tropical sites (925 and 926) different from those in middle and higher latitudes. The offsets between sites primarily reflect the biogeography, and to a smaller extent the temporal trends within the compositional data (Figure 5). Along CCA Axis 1, the samples are ordinated along a gradient from the northern North Atlantic to South Atlantic. CCA Axis 2 separates the tropical from higher-latitude sites in the North and South Atlantic. Axis 3 confirms common temporal trends at all sites. Similar ordinations are found when combining our data set with the subset of the Haq (1980) database (CCA and DCA runs 19; Figure S5). This confirms that the biogeographic and temporal gradients are robust within the Atlantic Ocean across the 17–11 Ma time interval. DCA Axis 1 sample scores appear to converge and indicate diminished site-to-site contrasts over time, although low-latitude versus high-latitude samples remain separated on DCA Axis 2 and 3 (Figure S6).

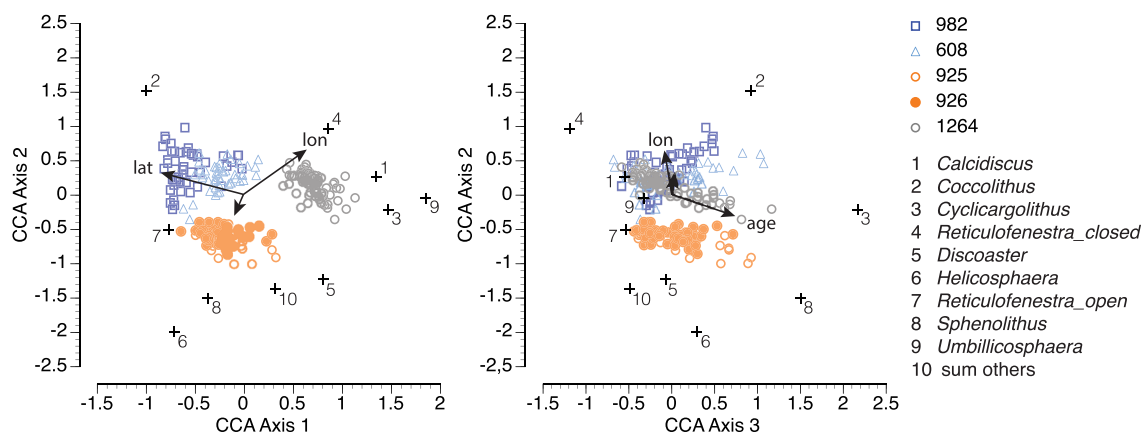


Figure 5. Canonical correspondence analysis (CCA) of genus-level census data for all sites combined. Scatter plots of taxon (+; numbers correspond to listed genera) and sample (colored symbols) scores on Axis 1 versus 2 and Axis 2 versus 3; latitude (lat), longitude (lon), and sample age served as environmental input variables.

Sites 925 and 926 hosted more taxa that are associated with warm, oligotrophic waters with a deep nutricline (as is the case today in the western equatorial Atlantic; Boeckel et al., 2006). During the MCO, midlatitude sites reflected similar “tropical” signatures with higher proportions of *Sphenolithus* (Site 608) and *Discoaster* (Site 1264), but these were significantly reduced during the MMCT (Figure 6b). Indeed, North Atlantic Site 608 holds both “tropical” and “high-latitude” characteristics. In the northern middle and high latitudes, *Coccilithus* had a stronghold, especially during the MCO (cf. Figures 5 and 6a), alternating with *Reticulofenestra* as the most common taxon. *Cyclicargolithus* was virtually absent in the highest northern latitude site (982) for the entire time interval but was most prominent in the South Atlantic (Site 1264) and shows distinct decreases across the MMCT (Figure 6c).

3.2.1. Intragenetic Diversity of *Reticulofenestrids*

Reticulofenestra was a common component in nearly all samples and reveals an overall increase in abundance across the investigated time interval at all sites (Figure 6c). The intragenetic diversity in this placolith-bearing group is highly variable (Text S3), with different morphospecies contributing to the long-term trends (Figure 7). It appears that medium (3–5 μm) to large (5–7 μm) morphospecies drive the steady increase across the MMCT. The largest morphospecies ($>7 \mu\text{m}$) start contributing significantly during the “icehouse” phase (from ~13–13.5 Ma), indicating a broadening of the size distribution within the group. The proportion of the smallest ($<3 \mu\text{m}$) placoliths is highly variable (Text S2), with distinct peak abundances within the MCO, MMCT, and post-MMCT at Site 982, and ~12–12.2 Ma at Sites 608, 925, and 926.

4. Discussion

4.1. Climate Change and Phytoplankton Fitness

At each sampled core depth, the nannofossil assemblages represent an average taxonomic composition over thousands of years—and ~50-fold that in terms of population generations. Therefore, we can assume that such averages represent species with high fitness, or at least species that remained within their ecological tolerances over long time intervals. As a result, ecological shifts in response to regional and submillennial scale climate change are difficult (if not impossible) to resolve in the fossil record. Instead, long-term migrations (habitat tracking cf. Haq, 1980) and species replacements, including speciation and extinction events, determine the observed assemblage changes. Here, we consider taxa that were most common and widespread over long time intervals, rather than a record of “true” species diversity. Species diversity is driven by rare, and often dissolution-prone taxa (Young et al., 2005), whereas the common groups provide the bulk of the algal biomass and primary production and are thus most relevant for climate-biota interactions and feedbacks (e.g., Hannisdal et al., 2012).

Marine primary productivity is generally enhanced in cooler surface waters of the high latitudes as well as in upwelling regions, where nutrient supply is increased through stronger vertical mixing and lateral advection. In the modern Atlantic, seasonal shifts in the position of the ITCZ (Figure 1), related to the strength

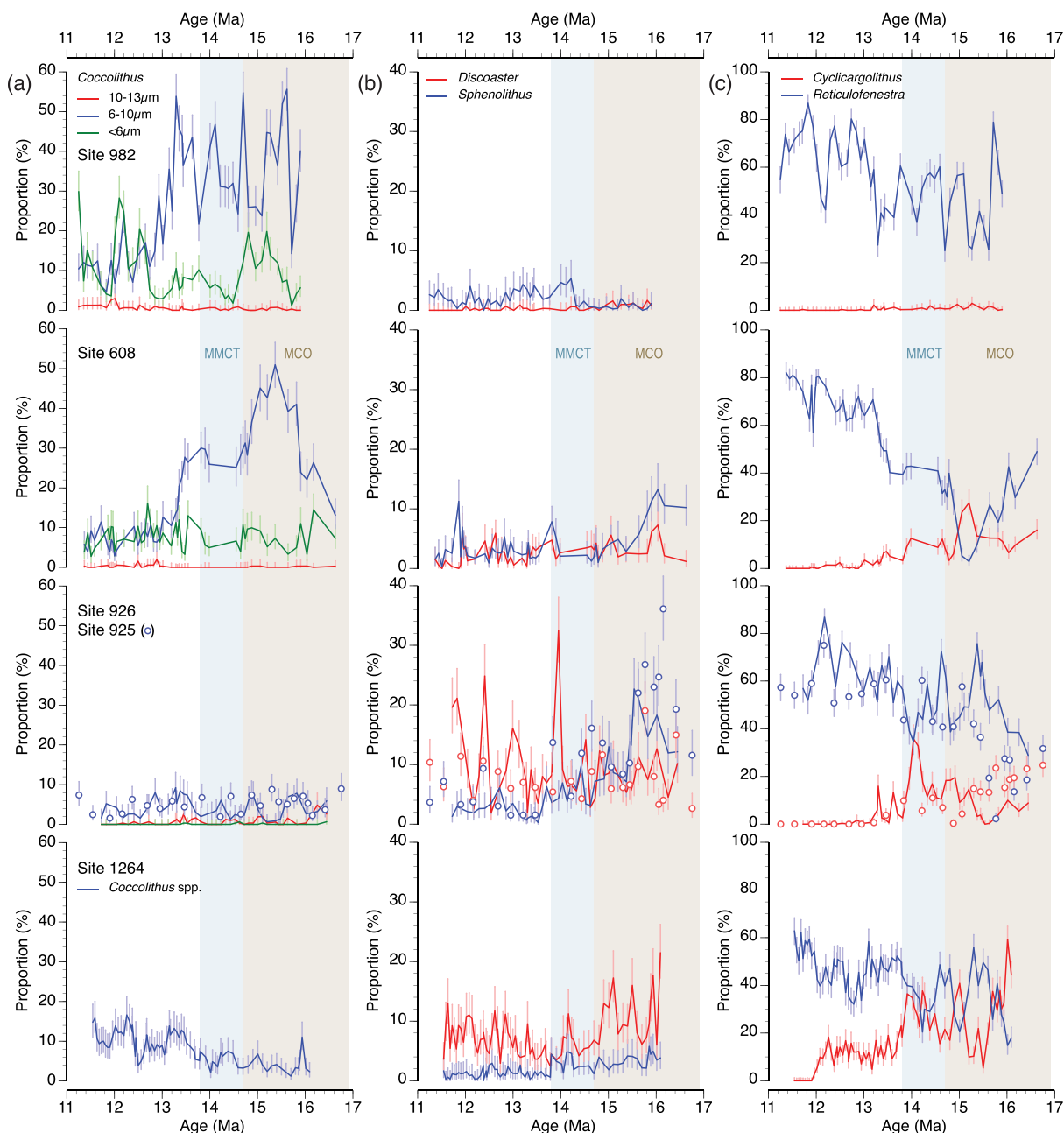


Figure 6. Middle Miocene time series of common calcareous nannofossil taxa across the Atlantic Ocean. The figure panels are arranged by latitude (from top to bottom: Site 982, 608, 925 + 926 (combined), and 1264) and show relative abundance (%) of (a) *Coccolithus pelagicus* (three size groups where determined); (b) *Discoaster* (red) and *Sphenolithus* (blue); (c) *Cyclargolithus* (red) and *Reticulofenestra* (blue; all morphospecies lumped; see Figure 7 for more details). Vertical error bars are 95% CI of census counts. Shaded areas indicate the MCO and MMCT time intervals.

of the SE and NE trade winds, affect the depth of the nutricline at tropical latitudes. When the SE trade winds are strongest during austral winter, the ITCZ reaches its northernmost position, and surface current transport in the South Atlantic leads to a deepening of the thermocline and nutricline in the western equatorial Atlantic, whereas the nutricline is uplifted in the eastern equatorial region (Boeckel et al., 2006). Whether such tropical east-west oceanographic contrasts may already have persisted during the Miocene is unclear. Nevertheless, the highest numbers of the warm water, oligotrophic taxon, *Sphenolithus* spp., were found at the equatorial Atlantic sites (Figures 6 and S5).

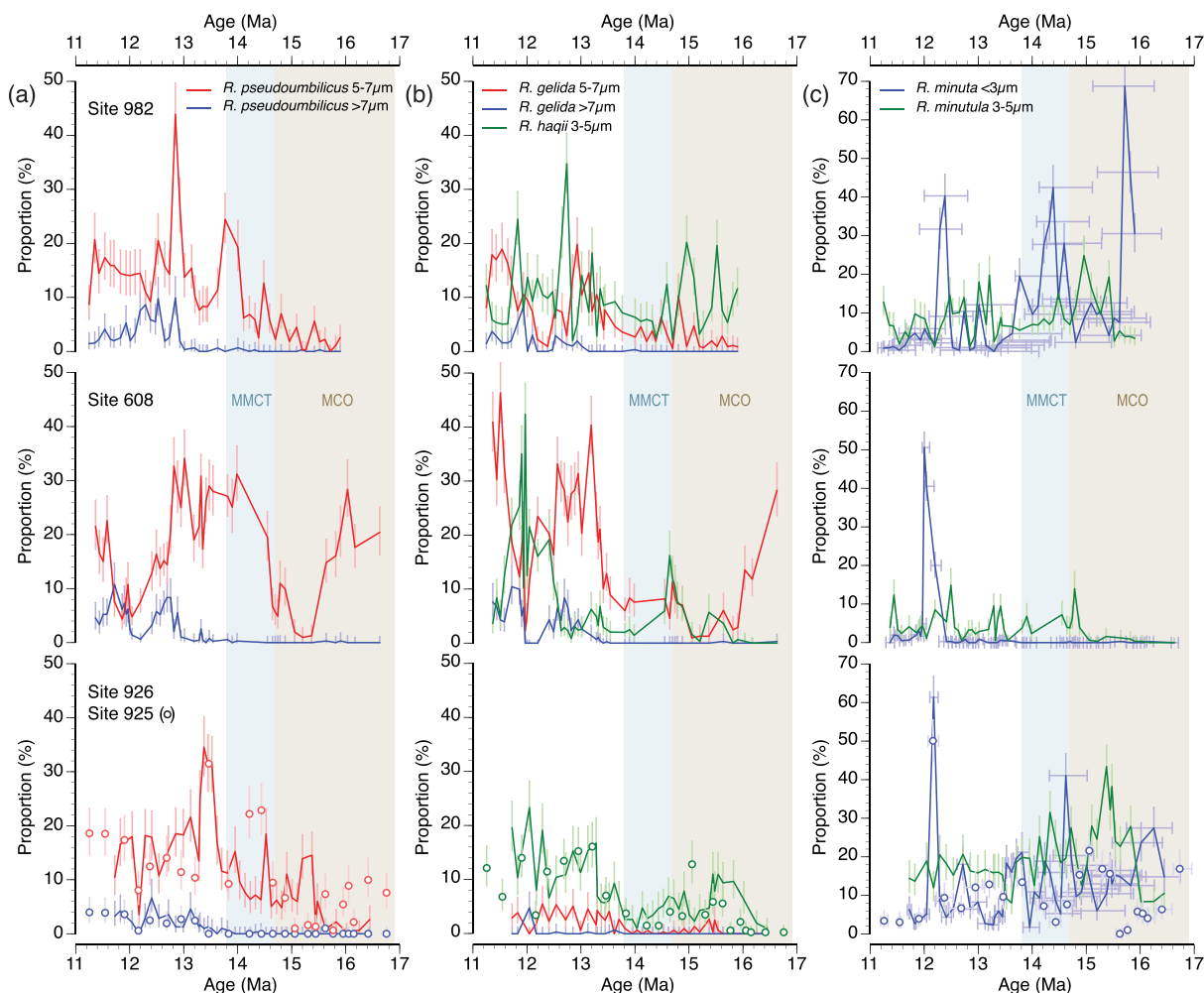


Figure 7. Proportional data (%) of total assemblage for different *Reticulofenestra* morphospecies. At Sites 982 (top), 608 (middle), and 925 and 926 (combined in bottom panels): (a) Size-defined morphotypes of *R. pseudoumbilicus*, 5–7 µm (red) and >7 µm (blue). (b) More heavily calcified *R. gelida* (5–7 and >7 µm; red and blue) and *R. haqii* (3–5 µm; green); (c) *R. minutula* (3–5 µm, larger central opening than *R. haqii*; green) and *R. minutula* (<3 µm; blue). Vertical error bars are 95% CI of census counts. To evaluate site-to-site correlations, the sample age constraints (68.2% range) are illustrated with horizontal error bars only in (c).

The modern, bipolar “icehouse” atmospheric and oceanographic circulation systems were not yet established during the middle Miocene (e.g., Holbourn et al., 2010), but we can draw some parallels in our analysis of the available paleoclimate and nannofossil proxy data. The warm (>28°C) surface temperatures of the extratropics during the MCO (Super et al., 2018) likely corresponded to more surface stratification and a deeper nutricline, as supported by the increased “tropical” nannofossil signatures at midlatitudes (Haq, 1980; this study). The lower pole-to-equator temperature gradient would have slowed down atmospheric circulation and ocean overturning and may also have contributed to less dispersal and increased the species compositional contrasts between Northern and Southern Hemisphere nannoplankton communities during this time (Figure 6).

Based on orbitally tuned, high-resolution stable benthic isotope records, the onset of the MMCT at ~14.6 Ma was characterized by relatively constant, low summer insolation over Antarctica and coincident with a distinct decrease in temperature and atmospheric CO₂ (Holbourn et al., 2005; Super et al., 2018; Figures 8a and 8b), which would have promoted ice sheet growth. Antarctic ice volume increased in distinct episodes of low eccentricity, which led to successive northward shifts in the ITCZ (Holbourn et al., 2010; Figure 8a). Following a third major step in ice growth ~13.8 Ma, midlatitude SSTs were consistently <28°C at Site 608, and paleo-pCO₂ levels remained below 400 ppmv (Super et al., 2018; Figure 8b), whereas SSTs in the

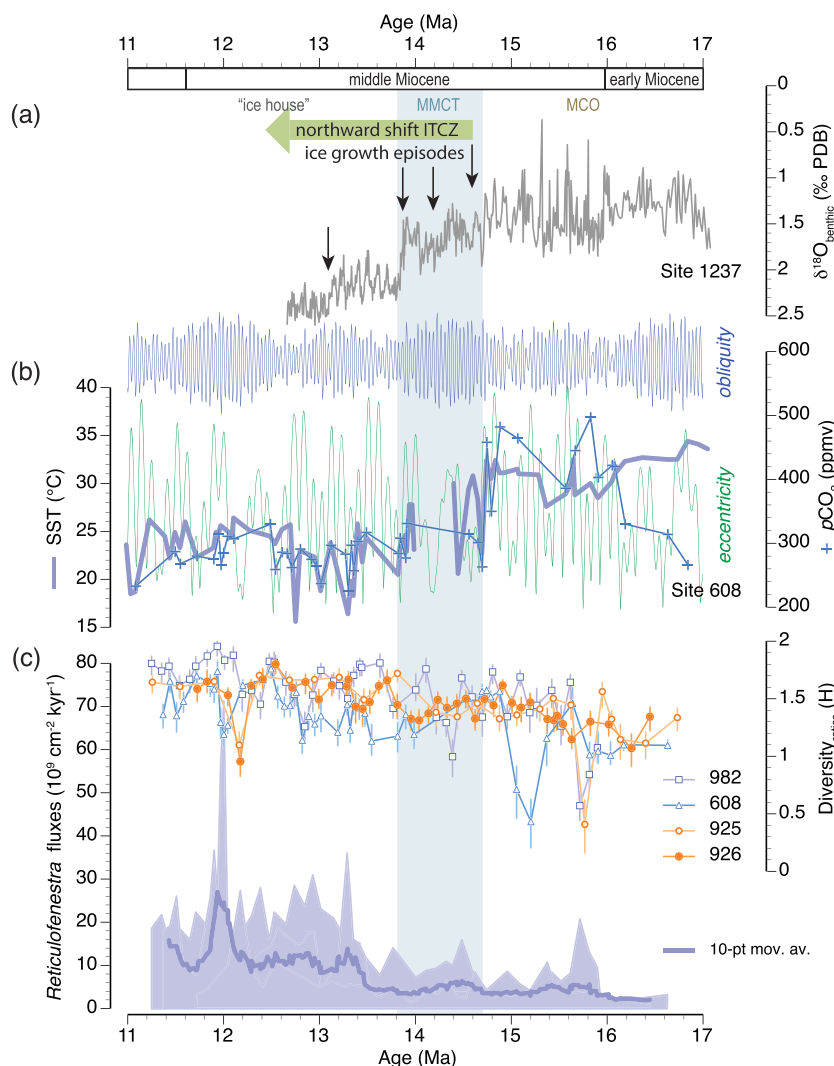


Figure 8. Comparison between paleoclimate and reticulofenestrid proxies across the MMCT. (a) Tuned record of benthic $\delta^{18}\text{O}$ at Site 1237 (Holbourn et al., 2005, 2007) in relation to obliquity (blue) and eccentricity (green) orbital solutions (Laskar et al., 2004, 2011); (b) Site 608 TEX₈₆-based SST (BAYSPAR 50th percentile; blue line) and average alkenone-derived pCO₂ estimates (plus symbols; Super et al., 2018); (c) Coccolith burial fluxes and morphospecies diversity within the Noelaerhabdaceae. Left axis: Blue line is a 10-pt moving average of *Reticulofenestra* coccolith fluxes for all sites combined, which are shown by the shaded area below (cf. Figure S8). Right axis: Shannon diversity index calculated for Noelaerhabdaceae only (including *Cyclicargolithus*; number of specimens per sample varies, $N = 74$ to 573). Low values (<1) indicate samples where one morphospecies dominates the fossil assemblage.

tropics remained $\sim 27^\circ\text{C}$ or higher (Foster et al., 2012; Zhang et al., 2013; Figure 2). The increased pole-to-equator temperature contrasts would have increased meridional overturning circulation and thus nutrient (re)cycling in the global oceans. The onset of coastal upwelling in the southern midlatitudes by ~ 10 Ma (Krammer et al., 2006; Rommerskirchen et al., 2011) exemplifies the progressive intensification and establishment of a modern oceanic overturn in the Atlantic since the MMCT. The site-specific DCA trends (Figures 3b and 4) most closely resemble the stable benthic isotope records, supporting that longer-term, whole-ocean changes underpin the observed phytoplankton composition shifts at all investigated sites, rather than an immediate effect of the stepwise cooling of the surface waters during the MMCT.

4.1.1. Paleoproductivity Indicators

Previous work has demonstrated that climate shifts during the MCO and MMCT did not lead to large changes in marine paleoproductivity in the Atlantic Ocean (Diester-Haass et al., 2009), although there is evidence for increased productivity across the MMCT in the tropical Pacific Ocean (Kochhann et al., 2017).

Patterns of benthic foraminiferal accumulation rates (Diester-Haass et al., 2009; Figure S7) do correspond to the gradual increase in nannofossil concentrations at the same locations. When converted into burial fluxes, a more distinct before-and-after MMCT scenario becomes evident; total nannofossil fluxes increased at all sites (Figure S8) and, on average, reticulofenestrid fluxes doubled after the MMCT (Figure 8c). A long-term increase in intrageneric morphospecies diversity (Figure 8c) points to diversification within the Noelaerhabdaceae as they became more ecologically prominent. It is possible that intensified dissolution during the MCO may have contributed to overall lower carbonate accumulation rates (Figure S3), but differential dissolution cannot explain the steady increase in large (5–7 and >7 μm), and thus dissolution resistant, *Reticulofenestra* morphospecies across and after the MMCT (Figures 7a and 7b).

We therefore conclude that the data support not only a significant increase in the relative abundance of reticulofenestrids within middle Miocene phytoplankton communities but also a diversification and an increase in their (export) production following the stepwise climate changes of the MMCT. Both observations indicate the high fitness of *Reticulofenestra* under the more variable climate dynamics of the “icehouse world” at all sites. It would appear that a threshold in fluxes was crossed at ~13.5 Ma, conspicuously close to the extinction event of *Sphenolithus heteromorphus* (13.53 Ma; defining the nannofossil biozone boundary NN6/NN5 of Martini, 1971, and CNM7/CNM8 of Backman et al., 2012). Evidently, the new “icehouse” climate state meant decreased fitness for some taxa. Even though SSTs in the tropical Atlantic did not change much, the fitness of typical “old warm world” taxa decreased, including *Cyclicargolithus* that flourished during the Oligocene and early Miocene (Haq, 1980; Plancq et al., 2013).

4.2. Evolutionary Overturn and Diversification Pulses

The post-MMCT increase in abundance and morphological diversification of *Reticulofenestra* (Figures 8c and 9c) can be seen as part of a series of similar global macroevolutionary overturn and species successions within the Noelaerhabdaceae family during the Neogene. In the Atlantic, Haq (1980) observed an earlier decline in *Cy. floridanus*—the dominant reticulofenestrid during the Oligocene and early Miocene—between 22.5 and 18 Ma (within NN2), followed by an increase in medium and larger reticulofenestrids (*R. haqii* and *R. pseudoumbilicus*). Plancq et al. (2013) identified the same species overturn also in the Pacific Ocean (DSDP Site 588) and postulated that a global cooling step, associated with early Miocene glaciations, could have triggered this initial decline in ecological prominence of *Cyclicargolithus*. Subsequently, other reticulofenestrids not only increased in abundance but also expanded their size range (diversified) from ~20.5–16.8 Ma (Henderiks & Pagani, 2007; Plancq et al., 2013). Here, our time series data add details to the final demise of *Cy. floridanus*, which although drastically decreased in numbers, remained a constant component in the South Atlantic and tropical sites until its last occurrence ~11.85 Ma (cf. Gradstein et al., 2012; Figure 9).

Both biotic and abiotic forcings impact species diversity (e.g., Ezard et al., 2011). The overall ecologies of reticulofenestrids were probably rather similar, as both *Cyclicargolithus* and *Reticulofenestra* were likely bloom-forming taxa (Plancq et al., 2013), but there are indications that *Reticulofenestra* had broader environmental tolerances than *Cyclicargolithus*, judging from their paleobiogeographic distribution during the middle Miocene (cf. Figure 6c). The ~7°C cooling and ~125 ppmv drop in pCO₂ during the MMCT (Super et al., 2018; Figures 9a and 9b) may have been a “final blow” to the fitness of *Cyclicargolithus* also in the middle and low latitudes of the South Atlantic. The time series at Sites 1264 and 926 (and to some extent Site 608) show anticorrelation in *Cyclicargolithus* and *Reticulofenestra* abundance during the MCO and MMCT, tentatively lending support that these taxa occupied the same niche and that *Reticulofenestra* was able to expand when *Cyclicargolithus* was drastically reduced after the MMCT. The gradual expansion of *Reticulofenestra* sizes, as the abundance of medium-large *Cyclicargolithus* was fading out (Figure 9c), also supports a scenario of species replacement following this stepwise change in global climate. Nevertheless, *Cyclicargolithus* was already virtually absent during the MCO at Site 982 and *Reticulofenestra* also expanded at these northern latitudes. Instead, the “high-latitude/cold water” (cf. Haq, 1980) genus *Coccolithus* steadily lost its ranking as dominant taxon (both in terms of relative abundance and burial fluxes) after the MMCT at Sites 608 and 982 (Figure 6a). Irrespective of other (phyto)plankton groups that may also have competed for resources, it is evident that the *Reticulofenestra* lineage increased its ecological prominence at all latitudes in the middle Miocene “icehouse world”.

Diversification pulses within the Noelaerhabdaceae, characterized by a gradual increase in maximum sizes and terminated by abrupt declines in size, have been documented across the Neogene (e.g., Beaufort, 1992;

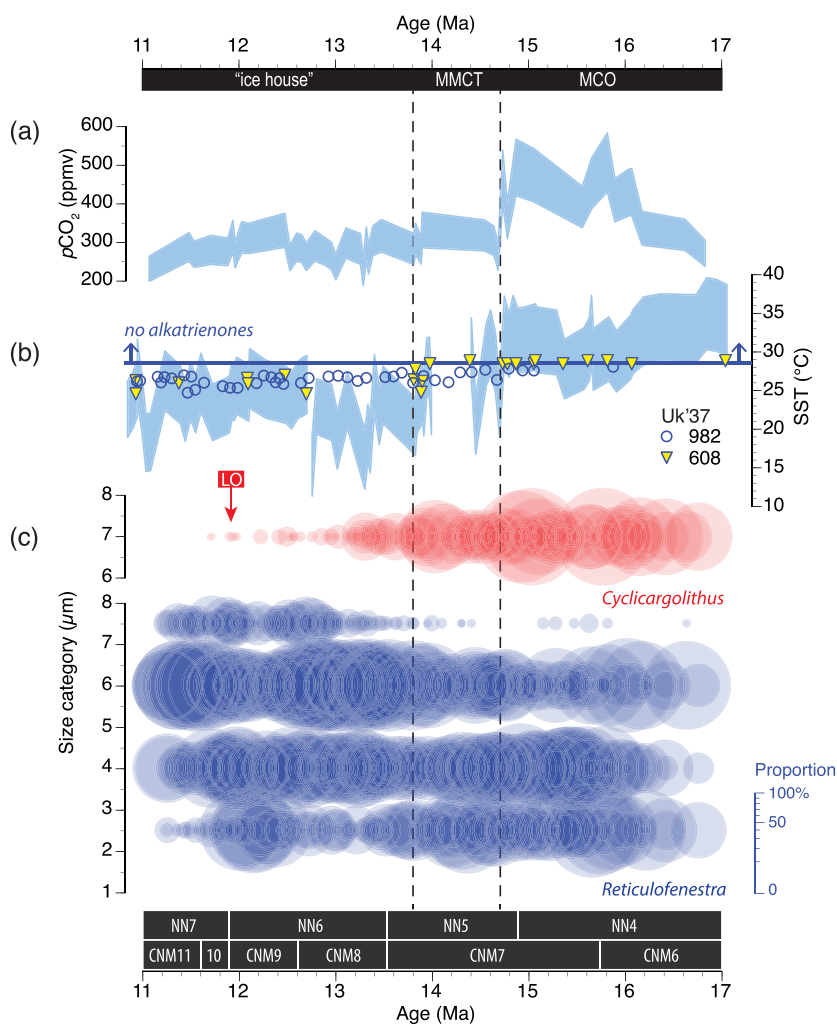


Figure 9. Stepwise climate change and macroevolution of reticulofenestrids during the middle Miocene. (a) Alkenone-derived $p\text{CO}_2$ and (b) TEX_{86} sea surface temperature estimates at Site 608 (blue shading is 68% CI; Super et al., 2018). Superimposed are U^{37}K SST estimates for Site 608 (triangles; Super et al., 2018) and Site 982 (circles; Herbert et al., 2016); note that these are close to this proxy's calibration maximum of 28.5°C . (c) Compilation of all samples from this study showing size categories of *Cy. floridanus* (red) and *Reticulofenestra* (blue; all morphospecies) as percentages (bubbles) within the subtotal of Noelaerhabdaceae. The last occurrence (LO) of *Cy. floridanus* falls within the top of nannofossil biozones NN6 (Martini, 1971) and CNM9 (Backman et al., 2012).

Bollmann et al., 1998; Bolton et al., 2016; Henderiks & Pagani, 2007; Imai et al., 2015; Matsuoka & Okada, 1990; Young, 1990). Recently, Bendif et al. (2019) demonstrated that such pulses reflect species radiations (speciation) separated by abrupt extinctions and that the three most recent pulses in the Pleistocene evolution of *Gephyrocapsa* (including *E. huxleyi*) are associated with step changes in global SST. These Pleistocene bursts in species diversification (“Matsuoka-Okada cycles”) had durations of ~ 0.5 Myr (Bendif et al., 2019), much shorter than those suggested by the Miocene data sets (e.g., Henderiks & Pagani, 2007; Imai et al., 2015; Young, 1990; this study). This could be due to a true acceleration of evolutionary rates (and related climatic forcings) during the Pleistocene compared to the Miocene. Alternatively, it could be an artifact of sampling resolution and the “coarser” and arbitrary size-based Miocene morphospecies definitions (Text S3), or other reasons, such as how we discern small morphological differences that may depict cryptic species (Sáez et al., 2003) in the fossil record.

The adaptability of the reticulofenestrids in the middle Miocene “icehouse” world was demonstrably high—but what could explain such competitive edge? Their wide biogeographic distribution and prominent presence at all investigated latitudes of the Atlantic suggests that middle Miocene *Reticulofenestra*

species had large population sizes and represented broad environmental tolerances (eurythermal and eurytrophic), similar to *E. huxleyi* today. Evolutionary genetic processes in such large and widespread populations may have led to a higher rate of adaptation, especially if interspecific hybridization and low-intensity gene flow occurred, as was demonstrated for Pleistocene *Gephyrocapsa* species (Bendif et al., 2019).

Noelaerhabdaceae are the only family of coccolithophores known to produce alkenones (Conte et al., 1995), long chain lipids that function as nutrient storage molecules (Eltgroth et al., 2005), and this may underpin the eurythermal and eurytrophic physiology of ancient reticulofenestrids (Brassell, 2014). More specifically, Brassell (2014) postulated that the first occurrence (and biosynthetic innovation) of alkatrienones after the Early Eocene Climatic Optimum (EECO; ~52 Ma) was related to the expansion of *Reticulofenestra* from high to lower latitudes and that this represents an adaptive response of this genus to a cooler climate at the time. In this rationale, storage lipids may be an advantage in surviving in a cooler ocean with higher environmental variability and seasonal constraints on productivity (Brassell, 2014). However, it is not unlikely that other cellular particulate organic matter (POM) could fulfill similar storage roles in other coccolithophores but that such soft tissue components are not preserved in sediments or lack the specific biomarker signatures that alkenones happen to provide.

Whether the production of alkenones would have provided *Reticulofenestra* with an (additional) competitive edge or not, the biosynthesis of alkatrienones appears to be linked to algal growth temperatures <28°C (Brassell, 2014, and references therein), resulting in an upper calibration limit for the alkenone-based U^{37}K SST proxy at ~28.5°C. Indeed, during the MCO, U^{37}K -based SST estimates at Site 608 are at this upper calibration limit (Super et al., 2018) and close to this limit at Site 982 (Herbert et al., 2016)—confirming the overall high SST in the higher northern latitudes, but also suggesting that alkatrienone biosynthesis came back online across and after the MMCT (Figure 9b).

Our understanding of how pCO_2 may impact the macroevolution of coccolithophores, and specifically reticulofenestrids, seems to have settled on distinct correlations between the levels of past atmospheric CO_2 and (mean) cell size (larger cells during times of higher pCO_2) (e.g., Bolton et al., 2016; Hannisdal et al., 2012; Henderiks & Pagani, 2008). Our new middle Miocene time series data suggest that the ~125 ppmv drop in pCO_2 (Super et al., 2018) at the start of the MMCT corresponds to a decrease in abundance of large-celled *Cy. floridanus* (and thus mean reticulofenestrid cell size) but that the subsequent, gradual increase of larger *Reticulofenestra* morphospecies (diversification and increase in mean cell size) was decoupled from the post-MMCT, lower “base level” of alkenone-derived pCO_2 (Figure 9a).

5. Conclusions

Our data reveal that calcareous nannoplankton assemblages tracked long-term climatic change during the middle Miocene and that the MMCT was a significant step toward establishing modern-like phytoplankton communities throughout the Atlantic Ocean. Typical “warm water” taxa were on the decline and eventually went extinct, whereas the abundance and diversity of eurythermal and eurytrophic reticulofenestrids steadily increased and even became dominant. High-latitude versus low-latitude compositional contrasts remained, similar to today, but all investigated sites saw the same macroevolutionary change within the reticulofenestrids. We explored what abiotic and biotic processes could underpin these patterns and conclude that the stepwise decrease in SST and pCO_2 across the MMCT presented a distinct shift in the adaptive landscape of marine phytoplankton, decreasing the fitness of some previously prominent species, such as *Cy. floridanus* and *Sphenolithus* (with high thermal optima) and demonstrating the high adaptability of the *Reticulofenestra* lineage to the new “baseline” conditions of the middle Miocene “icehouse world.” We speculate that a regression to a warmer state of the oceans may not negatively impact highly adaptable coccolithophore taxa, such as *E. huxleyi*, whose poleward expansion is already evident (Oziel et al., 2020; Rivero-Calle et al., 2015; Winter et al., 2014).

Data Availability Statement

Additional data figures and tables are provided in the supporting information. The raw data produced for this paper are publically available at the Zenodo data repository (Henderiks et al., 2020, <https://doi.org/10.5281/zenodo.3940622>) and at <https://doi.pangaea.de/10.1594/PANGAEA.921547>.

Conflict of Interest

There are no real or perceived financial conflict of interests for any author.

Acknowledgments

The authors are grateful to the IODP for providing the samples for this research and the staff members at the Bremen Core Repository (BCR) for help during the sampling visit. Uppsala University and the Swedish Research Council provided financial support (VR Grants 2011-4866 and 2016-04434 to J. H.). N. P.'s research contributions were made possible through a scholarship from the International Mobility Office of the Ecole Normale Supérieure de Lyon and the Région Auvergne-Rhône-Alpes (France) and an Erasmus Stage+ scholarship (EC). We thank Lucas Lourens for sharing unpublished data (tuned sample ages to compare age models at ODP Site 1264). Our reviewers, Isabella Raffi and Leah J. LeVay, are gratefully acknowledged for their time and helpful comments.

References

- Backman, J., & Raffi, I. (1997). Calibration of Miocene nannofossil events to orbitally tuned cyclostratigraphies from Ceara rise. In N. J. Shackleton, W. B. Curry, C. Richter, & T. J. Bralower (Eds.), *Proceedings of the Ocean Drilling Program, Scientific Results* (Vol. 154, pp. 83–99). College Station, TX: Ocean Drilling Program.
- Backman, J., Raffi, I., Rio, D., Fornaciari, E., & Pälike, H. (2012). Biozonation and biochronology of Miocene through Pleistocene calcareous nannofossils from low and middle latitudes. *Newsletters on Stratigraphy*, 47(2), 1–24.
- Badger, M. P. S., Lear, C. H., Pancost, R. D., Foster, G. L., Bailey, T. R., Leng, M. J., & Abels, H. A. (2013). CO₂ drawdown following the middle Miocene expansion of the Antarctic Ice Sheet. *Paleoceanography*, 28, 42–53. <https://doi.org/10.1002/palo.20015>
- Baumann, K.-H., Andruleit, H., Böckel, B., Geisen, M., & Kinkel, H. (2005). The significance of extant coccolithophores as indicators of ocean water masses, surface water temperature, and palaeoproductivity: A review. *Paläontologische Zeitschrift*, 79(1), 93–112.
- Beaufort, L. (1992). Size variations in Late Miocene *Reticulofenestra* and implication for paleoclimatic interpretation. *Memorie di Scienze Geologiche*, 43, 339–350.
- Bendif, E. M., Nevado, B., Wong, E. L. Y., Hagino, K., Probert, I., Young, J. R., et al. (2019). Repeated species radiations in the recent evolution of the key marine phytoplankton lineage *Gephyrocapsa*. *Nature Communications*, 10(1), 4234. <https://doi.org/10.1038/s41467-41019-12169-41467>
- Boeckel, B., Baumann, K.-H., Henrich, R., & Kinkel, H. (2006). Coccolith distribution patterns in South Atlantic and Southern Ocean surface sediments in relation to environmental gradients. *Deep-Sea Research Part I: Oceanographic Research Papers*, 53, 1073–1099.
- Bollmann, J., Baumann, K.-H., & Thierstein, H. R. (1998). Global dominance of *Gephyrocapsa* coccoliths in the Late Pleistocene: Selective dissolution, evolution or global environment change? *Paleoceanography*, 13(5), 517–529.
- Bolton, C. T., Hernández-Sánchez, M., Fuertes, M. A., González-Lemos, S., Abrevaya, L., Mendez-Vicente, A., et al. (2016). Decrease in coccolithophore calcification and CO₂ since the middle Miocene. *Nature Communications*, 7(1), 10284. <https://doi.org/10.1038/ncomms10284>
- Bordiga, M., Bartol, M., & Henderiks, J. (2015). Absolute nannofossil abundance estimates: Quantifying the pros and cons of different techniques. *Revue de Micropaleontologie*, 58(3), 155–165.
- Brassell, S. C. (2014). Climatic influences on the Paleogene evolution of alkenones. *Paleoceanography*, 29, 255–272. <https://doi.org/10.1002/2013PA002576>
- Broerse, A. T. C., Ziveri, P., van Hinte, J., & Honjo, S. (2000). Coccolithophore export production, species composition and coccolith-CaCO₃ fluxes in the NE Atlantic (34N 21W and 48N 21W). *Deep Sea Research, Part II*, 47, 1877–1905.
- Conte, M., Thompson, A., Eglington, G., & Green, J. C. (1995). Lipid biomarker diversity in the coccolithophorid *Emiliania huxleyi* (Prymnesiophyceae) and the related species *Gephyrocapsa oceanica*. *Journal of Phycology*, 31, 272–282.
- Curry, W. B., Shackleton, N. J., & Richter, C. (Eds.). (1995). Sites 925 and 926. *Proceedings of the Ocean Drilling Program, Initial Reports* (p. 154). College Station, TX: Ocean Drilling Program. <https://doi.org/10.2973/odp.proc.ir.154.1995>
- Diester-Haass, L., Billups, K., Gröcke, D. R., Francois, L., Lefebvre, V., & Emeis, K. C. (2009). Mid-Miocene paleoproductivity in the Atlantic Ocean and implications for the global carbon cycle. *Paleoceanography*, 24, PA1209. <https://doi.org/10.1029/2008PA001605>
- Elgtroth, M. L., Watwood, R. L., & Wolfe, G. V. (2005). Production and cellular localization of neutral long-chain lipids in the haptophyte algae *Isochrysis galbana* and *Emiliania huxleyi*. *Journal of Phycology*, 41(5), 1000–1009.
- Ezard, T. H. G., Aze, T., Pearson, P. N., & Purvis, A. (2011). Interplay between changing climate and species' ecology drives macroevolutionary dynamics. *Science*, 332, 349–351.
- Flower, B. P., & Kennett, J. P. (1993). Middle Miocene ocean-climate transition: High-resolution oxygen and carbon isotopic records from Deep Sea Drilling Project Site 588A, southwest Pacific. *Paleoceanography*, 8(6), 811–843.
- Flower, B. P., & Kennett, J. P. (1994). The middle Miocene climatic transition: East Antarctic ice sheet development, deep ocean circulation and global carbon cycling. *Palaeogeography, Palaeoclimatology, Palaeoecology*, 108, 537–555.
- Foster, G. L., Lear, C. H., & Rae, J. W. B. (2012). The evolution of pCO₂, ice volume and climate during the middle Miocene. *Earth and Planetary Science Letters*, 341, 243–254.
- Gartner, S. (1992). Miocene nannofossil chronology in the North Atlantic, DSDP Site 608. *Marine Micropaleontology*, 18(4), 307–331. [https://doi.org/10.1016/0377-8398\(1092\)90045-L](https://doi.org/10.1016/0377-8398(1092)90045-L)
- Gerecht, A. C., Šupraha, L., Edvardsen, B., Probert, I., & Henderiks, J. (2014). High temperature decreases the PIC/POC ratio and increases phosphorus requirements in *Coccolithus pelagicus* (Haptophyta). *Biogeosciences*, 11, 3531–3545.
- Gradstein, F. M., Ogg, J. G., Schmitz, M. D., & Ogg, G. M. (2012). *The geologic time scale 2012*, Amsterdam; Boston: Elsevier.
- Haidar, A. T., & Thierstein, H. (2001). Coccolithophore dynamics off Bermuda (N. Atlantic). *Deep Sea Research, Part II*, 48, 1925–1956.
- Hammer, Ø., & Harper, D. A. T. (2006). *Paleontological data analysis*, Oxford, UK: Wiley.
- Hammer, Ø., Harper, D. A. T., & Ryan, P. D. (2001). Past: Paleontological Statistics Software Package for education and data analysis. *Paleontologia Electronica*, 4, 1–9.
- Hannisdal, B., Henderiks, J., & Liow, L. H. (2012). Long-term evolutionary and ecological responses of calcifying phytoplankton to changes in atmospheric CO₂. *Global Change Biology*, 18(12), 3504–3516.
- Haq, B. U. (1980). Biogeographic history of Miocene calcareous nannoplankton and paleoceanography of the Atlantic Ocean. *Micropaleontology*, 26(4), 414–443. <https://doi.org/10.2307/1485353>
- Henderiks, J., Bartol, M., Pige, N., Karatsolis, B-T., & Lougheed, B. (2020). "Shifts in phytoplankton composition and stepwise climate change during the middle Miocene"—Age-depth models and calcareous nannofossil census data [data set]. Zenodo. <http://doi.org/10.5281/zenodo.3940622>
- Henderiks, J., & Pagani, M. (2007). Refining ancient carbon dioxide estimates: Significance of coccolithophore cell size for alkenone-based pCO₂ records. *Paleoceanography*, 22, PA3202. <https://doi.org/10.1029/2006PA001399>
- Henderiks, J., & Pagani, M. (2008). Coccolithophore cell size and the Paleogene decline in atmospheric CO₂. *Earth and Planetary Science Letters*, 269, 575–583.

- Herbert, T. D., Lawrence, K. T., Tzanova, A., Cleaveland-Peterson, L., Caballero-Gill, R., & Kelly, C. S. (2016). Late Miocene global cooling and the rise of modern ecosystems. *Nature Geoscience*, 9, 843–847. <https://doi.org/10.1038/NGEO2813>
- Herold, N., Huber, M., Müller, R. D., & Seton, M. (2012). Modeling the Miocene climatic optimum: Ocean circulation. *Paleoceanography*, 27, PA1209. <https://doi.org/10.1029/2008PA001605>
- Hilgen, F. J., Lourens, L. J., & van Dam, J. A. (2012). Chapter 29—The Neogene Period. In F. M. Gradstein, J. G. Ogg, B. Schmitz, & G. M. Ogg (Eds.), *The geologic time scale 2012* (pp. 923–978). Amsterdam; Boston: Elsevier.
- Hill, M. O., & Gauch, H. G. Jr. (1980). Detrended correspondence analysis: An improved ordination technique. *Vegetatio*, 42, 47–58.
- Holbourn, A., Kuhnt, W., Regenberg, M., Schulz, M., Mix, A., & Andersen, N. (2010). Does Antarctic glaciation force migration of the tropical rain belt? *Geology*, 38(9), 783–786.
- Holbourn, A., Kuhnt, W., Schulz, M., & Erlenkeuser, H. (2005). Impacts of orbital forcing and atmospheric carbon dioxide on Miocene ice-sheet expansion. *Nature*, 438(7067), 483–487. <https://doi.org/10.1038/nature04123>
- Holbourn, A., Kuhnt, W., Schulz, M., Flores, J.-A., & Andersen, N. (2007). Orbitally-paced climate evolution during the middle Miocene “Monterey” carbon-isotope excursion. *Earth and Planetary Science Letters*, 261(3), 534–550.
- Imai, R., Farida, M., Sato, T., & Iryu, Y. (2015). Evidence for eutrophication in the northwestern Pacific and eastern Indian oceans during the Miocene to Pleistocene based on the nannofossil accumulation rate, *Discoaster* abundance, and coccolith size distribution of *Reticulofenestra*. *Marine Micropaleontology*, 116, 15–27.
- Jansen, E., Raymo, M. E., & Blum, P. (Eds.) (1996). Site 982. *Proceedings of the Ocean Drilling Program, Initial Reports* (p. 162). College Station, TX: Ocean Drilling Program. <https://doi.org/10.2973/odp.proc.ir.162.1996>
- Kochhann, K. G. D., Holbourn, A., Kuhnt, W., Channell, J. E. T., Lyle, M., Shackford, J. K., et al. (2016). Eccentricity pacing of eastern equatorial Pacific carbonate dissolution cycles during the Miocene Climatic Optimum. *Paleoceanography*, 31, 1176–1192. <https://doi.org/10.1002/2016PA002988>
- Kochhann, K. G. D., Holbourn, A., Kuhnt, W., & Xu, J. (2017). Eastern equatorial Pacific benthic foraminiferal distribution and deep water temperature changes during the early to middle Miocene. *Marine Micropaleontology*, 133, 28–39.
- Krammer, R., Baumann, K.-H., & Henrich, R. (2006). Middle to late Miocene fluctuations in the incipient Benguela Upwelling System revealed by calcareous nannofossil assemblages (ODP Site 1085A). *Palaeogeography, Palaeoclimatology, Palaeoecology*, 230, 319–334.
- Laskar, J., Fienga, A., Gastineau, M., & Manche, H. (2011). La2010: A new orbital solution for the long-term motion of the earth. *Astronomy & Astrophysics*, 532, A89. <https://doi.org/10.1051/0004-6361/201116836>
- Laskar, J., Robutel, P., Joutel, F., Gastineau, M., Correia, A. C. M., & Levrard, B. (2004). A long-term numerical solution for the insolation quantities of the Earth. *Astronomy & Astrophysics*, 428(1), 261–285. <https://doi.org/10.1051/0004-6361:20041335>
- Lazarus, D., Barron, J., Renaudie, J., Diver, P., & Türke, A. (2014). Cenozoic planktonic marine diatom diversity and correlation to climate change. *PLoS ONE*, 9(1), e84857. <https://doi.org/10.1371/journal.pone.0084857>
- Leg 208 Shipboard Science Party (2004). Site 1264. In J. C. Zachos, D. Kroon, P. Blum, et al. (Eds.), *Proceedings of the Ocean Drilling Program, Initial Reports* (Vol. 208, pp. 1–73). College Station, TX: Ocean Drilling Program. http://www-odp.tamu.edu/publications/208_IR/VOLUME/CHAPTERS/IR208_05.PDF
- Levitus, S., Antonov, J. I., & Boyer, T. P. (2005). Warming of the world ocean, 1955–2003. *Geophysical Research Letters*, 32, L02604. <https://doi.org/10.1029/2004GL021592>
- Lohmann, G. P., & Carlson, J. J. (1981). Oceanographic significance of Pacific Late Miocene calcareous nannoplankton. *Marine Micropaleontology*, 6, 553–579.
- Lougheed, B. C., & Obrochta, S. P. (2019). A rapid, deterministic age-depth modeling routine for geological sequences with inherent depth uncertainty. *Paleoceanography and Paleoclimatology*, 34, 122–133. <https://doi.org/10.1029/2018PA003457>
- Lourens, L. J., Hilgen, F. J., Shackleton, N. J., Laskar, J., & Wilson, D. (2004). The Neogene Period. In F. Gradstein, J. Ogg, & A. Smith (Eds.), *A Geologic Time Scale* (pp. 409–452). Cambridge, United Kingdom: Cambridge Univ. Press.
- Martini, E. (1971). In A. Farinacci (Ed.), *Standard Tertiary and Quaternary calcareous nannoplankton zonation*, 2, (739–785). Rome: Proceedings of the 2nd International Conference Planktonic Microfossils.
- Matsuoka, H., & Okada, H. (1990). Time progressive morphometric changes of the genus *Gephyrocapsa* in the Quaternary sequence of the tropical Indian Ocean, Site 709. *Proceedings ODP, Scientific Research*, 115, 225–270.
- Oziel, L., Baudena, A., Ardyna, M., Massicotte, P., Randelhoff, A., Sallée, J.-B., et al. (2020). Faster Atlantic currents drive poleward expansion of temperate phytoplankton in the Arctic Ocean. *Nature Communications*, 11(1), 1–8. <https://doi.org/10.1038/s41467-020-15485-5>
- Pälike, H., Lyle, M. W., Nishi, H., Raffi, I., Ridgwell, A., Gamage, K., et al. (2012). A Cenozoic record of the equatorial Pacific carbonate compensation depth. *Nature*, 488(7413), 609–614. <https://doi.org/10.1038/nature11360>
- Plancq, J., Mattioli, E., Henderiks, J., & Grossi, V. (2013). Global shifts in Noelaerhabdaceae assemblages during the late Oligocene-early Miocene. *Marine Micropaleontology*, 103, 40–50.
- Raffi, I., Backman, J., Fornaciari, E., Pälike, H., Rio, D., Lourens, L., & Hilgen, F. (2006). A review of calcareous nannofossil astrobiogeochronology encompassing the past 25 million years. *Quaternary Science Reviews*, 25, 3113–3137.
- Rivero-Calle, S., Gnanadesikan, A., Del Castillo, C. E., Balch, W. M., & Guikema, S. D. (2015). Multidecadal increase in North Atlantic coccolithophores and the potential role of rising CO₂. *Science*, 350, 1533–1537.
- Rommerskirchen, F., Condon, T., Mollenhauer, G., Dupont, L., & Scheffuss, E. (2011). Miocene to Pliocene development of surface and subsurface temperatures in the Benguela Current system. *Paleoceanography*, 26, PA3216. <https://doi.org/10.1029/2010PA002074>
- Ruddiman, W. F., & Heezen, B. C. (1967). Differential solution of planktonic foraminifera. *Deep Sea Research and Oceanographic Abstracts*, 14(6), 801–808. [https://doi.org/10.1016/S0011-7471\(106\)80016-80010](https://doi.org/10.1016/S0011-7471(106)80016-80010)
- Ruddiman, W. F., Kidd, R. B., Thomas, E., Baldauf, J. G., Clement, B. M., Dolan, J. E., et al. (1987). Site 608, *Initial Reports DSDP* (94). Washington, DC: U.S. Government Printing Office.
- Sáez, A. G., Probert, I., Geisen, M., Quinn, P., Young, J., & Medlin, L. K. (2003). Pseudo-cryptic speciation in coccolithophores. *Proceedings of the National Academy of Sciences of the United States of America*, 100(12), 7163–7168.
- Sarmiento, J. L., Slater, R., Barber, R., Bopp, L., Doney, S. C., Hirst, A. C., et al. (2004). Response of ocean ecosystems to climate warming. *Global Biogeochemical Cycles*, 18, GB3003. <https://doi.org/10.1029/2003GB002134>
- Savin, S., Abel, L., Barrera, E., Hodell, D., Keller, G., Kennett, J. P., et al. (1985). The evolution of Miocene surface and near surface marine temperatures: Oxygen isotope evidence. In J. P. Kennett (Ed.), *The Miocene Ocean: Paleoceanography and biogeography, Memoir of the Geological Society of America* (Vol. 163, pp. 49–82). Boulder, CO: The Geological Society of America. <https://doi.org/10.1130/MEM163-p49>

- Shevenell, A. E., Kennett, J. P., & Lea, D. W. (2004). Middle Miocene Southern Ocean cooling and Antarctic cryosphere expansion. *Science*, 305(5691), 1766–1770. <https://doi.org/10.1126/science.1100061>
- Stoll, D. K., Guitian, J., Hernandez-Almeida, I., Mejia, L. M., Phelps, S., Polissar, P., et al. (2019). Upregulation of phytoplankton carbon concentrating mechanisms during low CO₂ glacial periods and implications for the phytoplankton pCO₂ proxy. *Quaternary Science Reviews*, 208, 1–20. <https://doi.org/10.1016/j.quascirev.2019.01.012>
- Suchéras-Marx, B., Escarguelb, G., Ferreira, J., & Hammer, Ø. (2019). Statistical confidence intervals for relative abundances and abundance based ratios: Simple practical solutions for an old overlooked question. *Marine Micropaleontology*, 151, 101751.
- Suchéras-Marx, B., & Henderiks, J. (2014). Downsizing the pelagic carbonate factory: Impacts of calcareous nannoplankton evolution on carbonate burial over the past 17 million years. *Global and Planetary Change*, 123, 97–109.
- Super, J. R., Thomas, E., Pagani, M., Huber, M., O'Brien, C., & Hull, P. M. (2018). North Atlantic temperature and pCO₂ coupling in the early-middle Miocene. *Geology*, 46(6), 519–522.
- Šupraha, L., Gerecht, A. C., Probert, I., & Henderiks, J. (2015). Eco-physiological adaptation shapes the response of calcifying algae to nutrient limitation. *Scientific Reports*, 5, 16,499. <http://www.nature.com/articles/srep16499>
- Ter Braak, C. J. F. (1986). Canonical correspondence analysis: A new eigenvector technique for multivariate direct gradient analysis. *Ecology*, 67, 1167–1179.
- Thomas, M. K., Kremer, C. T., Klausmeier, C. A., & Litchman, E. (2012). A global pattern of thermal adaptation in marine phytoplankton. *Science*, 338(6110), 1085–1088. <https://doi.org/10.1126/science.1224836>
- Winter, A., Henderiks, J., Beaufort, L., Rickaby, R. E. M., & Brown, C. W. (2014). Poleward expansion of the coccolithophore *Emiliania huxleyi*. *Journal of Plankton Research*, 36, 316–325.
- Woodruff, F., & Savin, S. M. (1991). Mid-Miocene isotope stratigraphy in the deep sea: High-resolution correlations, paleoclimatic cycles, and sediment preservation. *Paleoceanography*, 6(6), 755–806.
- Wright, J. D., Miller, K. G., & Fairbanks, R. G. (1992). Early and Middle Miocene stable isotopes: Implications for Deepwater circulation and climate. *Paleoceanography*, 7(3), 357–389.
- Young, J. (1990). Size variation of Neogene *Reticulofenestra* coccoliths from Indian Ocean DSDP cores. *Journal of Micropaleontology*, 9(1), 71–86.
- Young, J., Geisen, M., & Probert, I. (2005). A review of selected aspects of coccolithophore biology with implications for paleobiodiversity estimation. *Micropaleontology*, 51(4), 267–288.
- Zeeden, C., Hilgen, F., Westerhold, T., Lourens, L., Röhl, U., & Bickert, T. (2013). Revised Miocene splice, astronomical tuning and calcareous plankton biochronology of ODP Site 926 between 5 and 14.4 Ma. *Palaeogeography, Palaeoclimatology, Palaeoecology*, 369, 430–451.
- Zhang, Y. G., Pagani, M., Liu, Z., Bohaty, S., & DeConto, R. (2013). A 40-million-year history of atmospheric CO₂. *Philosophical Transactions of the Royal Society B*, 371.

References From the Supporting Information

- Backman, J. (1980). Miocene-Pliocene nannofossils and sedimentation rates in the Hatton-Rockall Basin, NE Atlantic Ocean. *Stockholm Contributions in Geology*, 36(1), 91.
- King, T. A., Ellis, W. G., Murray, D. W., Shackleton, N. J., & Harris, S. (1997). Miocene evolution of carbonate sedimentation at the Ceara Rise: A multivariate data/proxy approach. In N. J. Shackleton, W. B. Curry, C. Richter, & T. J. Bralower (Eds.), *Proc. ODP, Sci. Results, 154* (pp. 349–365). College Station, TX: Ocean Drilling Program. <https://doi.org/10.2973/odp.proc.ir.162.1996>
- Langer, G., Nehrk, G., & Jansen, S. (2007). Dissolution of *Calcidiscus leptoporus* coccoliths in copepod guts?—A morphological study. *Marine Ecology Progress Series*, 331, 139–146.
- Matsuoka, H. (1990). A new method to evaluate dissolution of CaCO₃ in the deep-sea sediments. *Transactions and Proceedings. Paleontological Society of Japan*, 157, 430–434.